A study of the non-uniformity of the PMT photocathode response and its influence on the results obtained in different scintillation counting experiments

V. Todorov, Philippe Cassette, Ch. Dutsov, Benoit Sabot, S. Georgiev, K. Mitev

A Study of the Non-uniformity of the PMT Photocathode Response and its Influence on the Results Obtained in Different Scintillation Counting Experiments

V. Todorov[a,*], P. Cassette[a], Ch. Dutsov[b], B. Sabot[c], S. Georgiev[a], K. Mitev[a]

[a] *Sofia University "St. Kliment Ohridski" James Bourchier Blvd, 1164 Bulgaria, Sofia*
[b] *Paul Scherrer Institute, Villigen PSI, 5232, Switzerland*
[c] *Universite Paris-Saclay, CEA, LIST, Laboratoire National Henri Becquerel (LNE-LNHB), F-91120, France*

Abstract

This work presents an investigation on the non-uniformity of the response of the photocathode of two photomultiplier tubes (PMTs) and its potential influence on the results of scintillation measurements. An experimental system was developed which allows studies of the non-uniformity of the photocathode response and its influence on the shape of alpha spectra obtained after pulse-shape discrimination. The system is presented together with tests of Hamamatsu R7600U-200 and H11934-203 PMTs. A degradation of the counting efficiency and a shift of the peak position towards smaller values were identified in the measurements near the edges of the photocathode where the energy resolution is significantly worse compared to the central region of the PMT. Such non-uniformity also affects absolute activity measurements based on the free parameter model, i.e., the Triple to Double Coincidence Ratio and the CIEMAT/NIST efficiency tracing methods. A significant non-uniformity of the response of a PMT would interfere with the assumption of the traditional free parameter model of a Poisson distribution of the number of emitted photons. Experimental results are presented in the paper, together with a discussion of

*V. Todorov
Email address: vladislav.todorow@gmail.com (V. Todorov)

their practical influence on scintillation and absolute activity measurements.

Key words: Photocathode response spatial non-uniformity, plastic scintillation spectrometry, energy resolution, radon measurements, pulse-shape discrimination

1. Introduction

The spatial non-uniformity of the response of photomultiplier tubes has been studied in the past [1, 2] and has been identified as one of the factors that can deteriorate the energy resolution in scintillation spectrometry [3–5]. In Ref. [6], after a direct measurement, the position-dependent quantum efficiency of the photocathode is implemented in a Monte Carlo light transport code to study the energy resolution in scintillation measurements and a decrease of 11% in the energy resolution is observed. In a recent study [7] we have shown that, when analyzing alpha spectra obtained after pulse-shape discrimination (PSD) in measurements with plastic scintillators, the shape of the alpha peaks is distorted if there is a significant non-uniformity of the PMT response.

In general, the majority of the studies of the non-uniformity of the photocathode response are directed towards PMTs with large area photocathodes [8–10] with some indicating a relative difference in photocathode efficiency as much as 40 – 50% [11].

The objective of this work was to develop an experimental system allowing quantification of the non-uniformity of the photocathode response of the PMTs and to study the influence of this non-uniformity on various scintillation measurements like: the analysis of alpha spectra obtained after pulse-shape discrimination and the absolute activity measurements using the free parameter model in liquid scintillation counting [12].

2. Methods and materials

In this paper, the response of the photocathode of two PMTs – Hamamatsu R7600U-200 and Hamamatsu H11934-203 is studied. Both PMTs have a metal

channel dynode structure with 10 stages in the R7600U-200 PMT and 12 in the H11934. Both PMTs have identical glass window size but significantly different effective area of the photocathode (see Fig. 1).

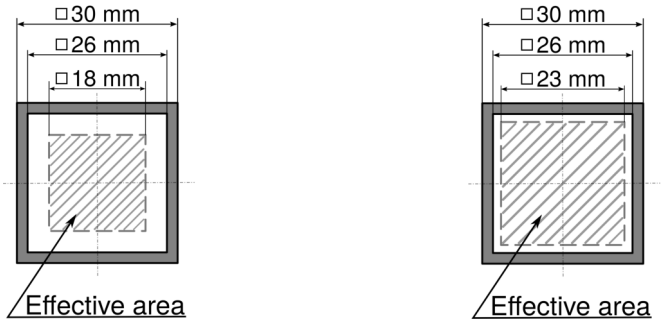

Figure 1: Size of the outer casing, the photocathode and the effective area of the R7600U-200 (left) [13] and H11934-200 (right) [14] PMT

In previous works, a significant non-uniformity of the photocathode response was identified in the Hamamatsu R7600-00-M4 PMTs [15] which have similar characteristics to R7600U-200. To the best of our knowledge, there are no published results for the photocathode non-uniformity response of Hamamatsu H11934-203.

In order to study the non-uniformity of photocathode response of the Hamamatsu H11934-203 and R7600U-200 PMTs, two experimental systems were built. The first system, shown schematically in Fig. 2, consists of a homemade LED pulser (see Fig. 3), printed gray filters for adjusting the light intensity, a holder for neutral density (ND) filters with certified transmission (Thorlabs NDK01), a fiber collimator followed by a multimode optical fiber with a 200 μm core diameter.

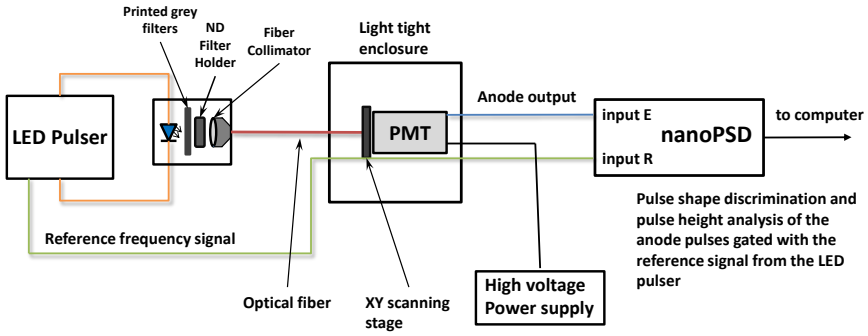

Figure 2: Experimental setup for studying the non-uniformity of the PMTs photocathode response.

During the scans, the printed filters are fixed and no ND filters are placed in the holder. The fiber collimator collimates the light from the LED on one end of the optical fiber. The other end is touching the PMT window. The minimum step of the scanning stage is 0.1 mm in each direction which is achieved with a micrometer screw.

Using the coincidence counting functionality of the nanoPSD device [16], the anode signal of the PMTs is analyzed in coincidence with the reference frequency signal produced by the LED pulser. The ND filters are used for studying the linearity of PMT response by varying the intensity of the incident light on the photocathode. The acquisition time for each point in all scans is 30 seconds.

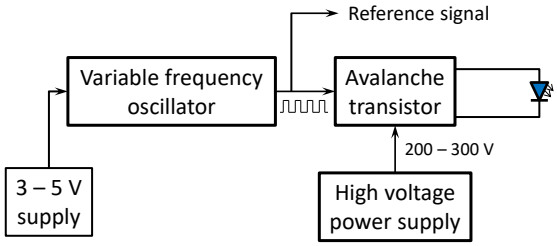

Figure 3: A scheme of the homemade LED pulser used in the experimental setup. An LED (405 nm wavelength) is powered by a fast switching signal with frequency governed by the variable frequency oscillator. The transistor works in an avalanche mode and the time constant of the switch is about 0.25 ns.

The second developed system is shown in Fig. 4. This system is designed for measuring the alpha spectra from the PSF200A plastic scintillator (PS) with ^{222}Rn absorbed in it. It consists of a 3D printed holder for the PMT and a 4×4 grid which is firmly fixed on top of the PMT window. The distance between the outermost edges of the grid is 26 mm. This ensures that the PS would be positioned within the glass window of the PMT. In order to reduce the photon loss, the PS piece ($3 \times 3 \times 5$ mm^3) is enveloped in reflective foil (3M Enhanced Specular Reflector) and fixed in a 3D printed plastic holder (5×5 mm^2). A thin layer of silicon optical grease is applied between the scintillator and the reflective foil. Optical grease is also deposited between the scintillator and the PMT window. The PSF200A scintillator has excellent α/β pulse-shape discrimination capabilities [17], which enabled us to study the changes in the alpha spectra of ^{222}Rn and its decay products when placing the scintillator at different positions of the grid.

Figure 4: Left: the grid fixed on the holder of the H11934 PMT; Center: the plastic scintillator piece inserted in a holder covered with reflective foil; Right: the PS holder slides through each hole in the grid ensuring that the PS touches the PMT window.

The radioactive noble gas ^{222}Rn has useful properties for studying both the PSD capabilities and energy resolution of plastic scintillators. Radon can diffuse in the PS matrix [17], where it can undergo alpha decay ($E_{\alpha,Rn-222} = 5.489$ MeV) with a half-life of 3.823(5) days. ^{222}Rn has four short-lived decay products: two beta emitters (^{214}Bi and ^{214}Pb) and two alpha emitters – ^{218}Po ($E_{\alpha,Po-218} = 6.002$ MeV) and ^{214}Po ($E_{\alpha,Po-214} = 7.686$ MeV). The emitted alpha particles have a short range, so most of the α particles dissipate all their energy in the scintillator. However, due to the non-uniformity of the response

of the photocathode, variations in both the PSD and pulse-height spectra of the alpha particles are expected.

The signal processing is accomplished with the nanoPSD analyzer again. The pulse-shape discrimination is based on ballistic deficit measurement and digital time-invariant pulse shaping. The PMT signal is passed through slow and fast shapers. Then the pulse-height of each shaped signal is measured using peak detectors. The Time-Invariant Pulse-shape Signature (TIPS) is defined as the ratio of the maximum of the slow shaper and the maximum of the fast shaper [18]. Four spectra are obtained simultaneously: one PSD (TIPS) spectrum, and three pulse-height spectra: the raw pulse-height spectrum (α+β) and the separated alpha and beta spectra. An example of the real-time acquisition spectra is given in Fig. 5. More details regarding the implementation of the method for pulse-shape discrimination can be found in [18].

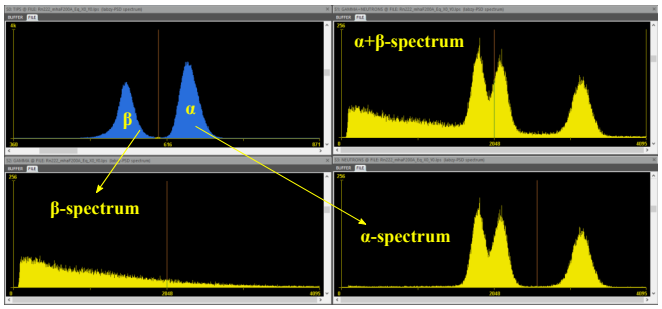

Figure 5: The nanoPSD program interface showing all four spectra. Top left: the PSD spectrum; top right: the raw pulse-height spectrum; bottom: the separated beta (left) and alpha (right) spectra.

3. Results

3.1. Fine-step scanning of the photocathode

In this part of the study of the photocathode response, both H11934 and R7600U PMTs were scanned using the system shown in Fig. 2. Each PMT had a dedicated 3D printed holder which secured the PMT during the scans. A close-up photo of the PMT window and the frame of reference used for the

scans are shown in Fig. 6. From here on, the focusing electrodes of the PMTs, visible through the glass window, would be referred as 'strips'.

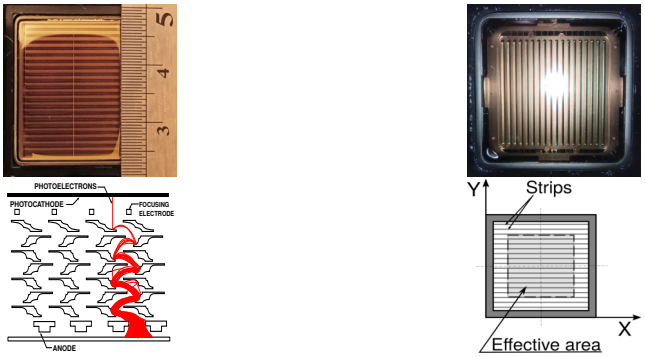

Figure 6: Top left: Photo of the H11934 PMT window; Top right: Photo of the R7600U PMT window; Bottom left: Transversal view of the metal channel dynode structure [19]; Bottom right: A frame of reference used for the scans (x-axis along the strips and y-axis across the scrips).

3.1.1. Scans of Hamamatsu H11934-203 PMT

Figure 7 shows the scans along the strips of the H11934 PMT. The high voltage applied to the H11934 PMT during the scans is set to +1000 V. The slow and fast thresholds of the nanoPSD are both set to avoid noise pulses and printed grey filters were used to decrease the intensity of the LED light. The variation in the centroid position of the LED pulser peak is about 15% in the effective area of the photocathode (23×23 mm^2) but can be much greater in some scans. For example, for Y=8 mm, the relative difference between the maximum and minimum value is 33%. The clear peak visible in the central region along the strips of the PMT is due to a central wire in the middle of the PMT perpendicular to the strips (see Fig. 6 top left). It should be noted, however, that in another study [20] the area around the central wire of Hamamatsu H5783-06 PMT was found to decrease the photocathode response.

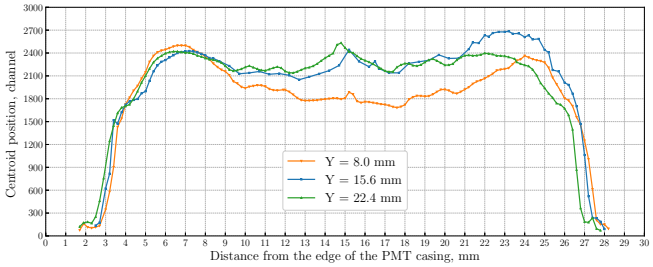

Figure 7: Peak centroid position vs position along the strips of the H11934 PMT.

Figure 8 shows the scans with the LED across the strips of H11934 PMT.

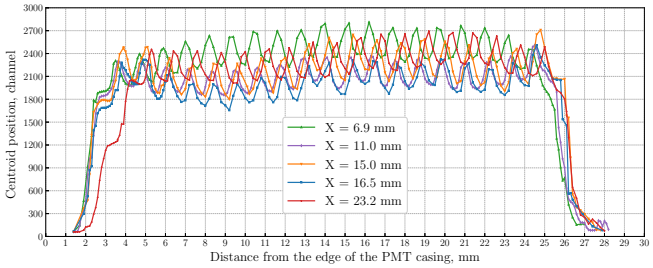

Figure 8: Peak centroid position vs position across the strips of the H11934 PMT.

Clearly, those scans reveal that the response of the PMT significantly depends on the position of the incident photons in the effective area of the photocathode. The observed periodic changes in the response can undoubtedly be attributed to the focusing electrodes of the PMT. However, the minimum and maximum values of the photocathode response are different along a single scan. This suggests that the photocathode response is also modulated by factors other than the multiplication structure of the PMT.

3.1.2. Scans of Hamamatsu R7600U-200 PMT

Figure 9 shows the scans with the R7600U PMT along the strips. For these scans, the high voltage supply is set to +850 V.

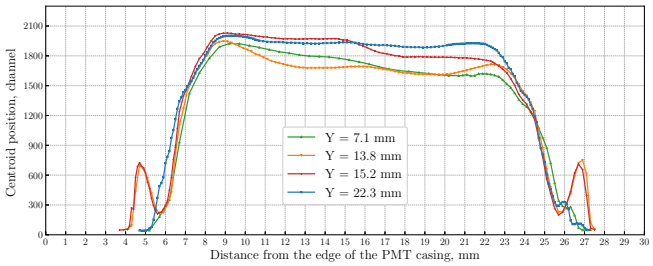

Figure 9: Peak centroid position vs position along the strips of the R7600U PMT.

The variation between the maximum and minimum of the peak position is up to 17% in the effective area of the photocathode (18×18 mm^2). There are some noticeable peaks outside the effective area in the scans at Y=13.8 and 15.2 mm which could be caused by the metal attachments in the center of the first dynode (see Fig. 6, top right).

Scans across the strips of the R7600U PMT are presented in Figure 10. Similarly to the H11934 PMT, those scans reveal the internal structure of the PMT quite well and the response varies between two peaks (or two valleys).

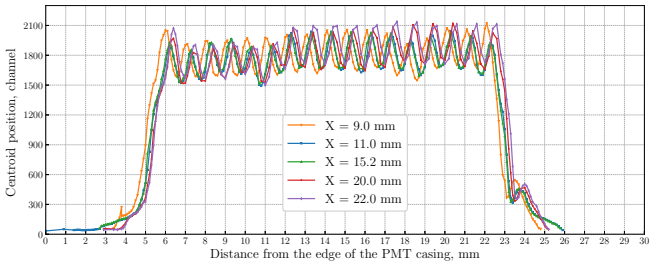

Figure 10: Peak centroid position vs position across the strips of the R7600U PMT.

There is a small peak at about 24 mm present in all scans and at X = 11, 15.2, 20.0 and 22.0 mm and a drop appears at 11 mm. However, by viewing the PMT window it is difficult to unambiguously identify the cause of these changes.

3.2. Linearity of the light intensity response of the studied PMTs

To study the linearity of the light intensity response we made measurements with optical filters with certified transmission (Thorlabs Neutral Density filters) which are placed after the printed grey filters (see Fig. 2). Figure 11 shows the LED spectra obtained after attenuating the light with ND filters with different optical transmission.

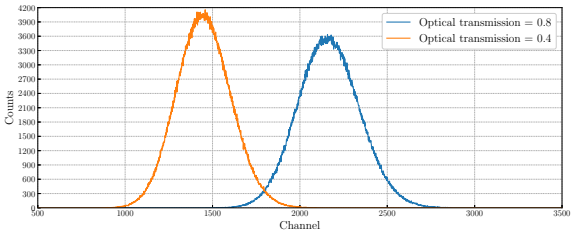

Figure 11: Peak position in the spectra after different attenuation of the LED light with ND filters. The optical transmission of the filters is 0.8 and 0.4.

3.2.1. Linearity study of the H11934-203 PMT

Figure 12 presents measurements with 7 different filters at one position on the effective area of the H11934 PMT with the supply voltage set to +1000 V.

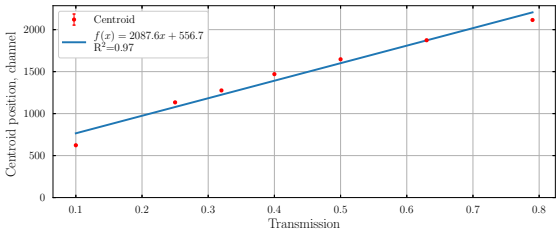

Figure 12: Peak centroid position vs. light intensity for the H11934 PMT at +1000 V. The spectrum range is 4096 channels.

With the high voltage set to the maximum rating for this PMT, a non-linearity in the response of the PMT is observed. This could be attributed to saturation of the PMT divider response. Therefore, the output current ceases to be proportional to the intensity of the incident light. The effect is known and discussed in [19].

When the supply voltage is decreased to +750 V, which leads to lower anode current, the response of the PMT becomes linear (Fig 13).

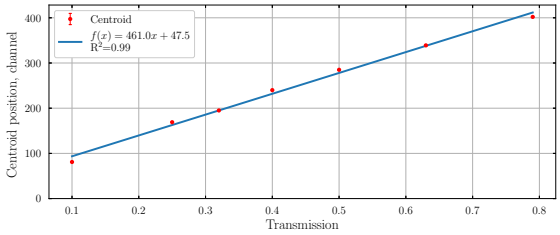

Figure 13: Peak centroid position vs. light intensity for the H11934 PMT at +750 V. The spectrum range is 512 channels.

A significant spread of the experimental points is observed for measurements at random positions on the effective area of the photocathode (Fig 14). The contribution of the photocathode non-uniformity results in big dispersion between measurements even with the same optical filter (compare Fig. 14 to Fig. 13). Moreover, the deviation would be more pronounced if measurements outside the effective area of the PMT are also included (not shown here).

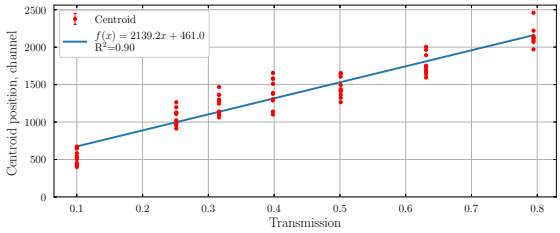

Figure 14: Peak centroid position vs. light intensity for the H11934 PMT at +1000 V. Points corresponding to the same optical transmission are measured on ten different random positions in the effective area of the photocathode. The spectrum range is 4096 channels.

3.2.2. Linearity study of the R7600U-200 PMT

Figure 15 presents the results from the linearity study of the R7600U PMT. Similarly to the H11934 PMT, non-linearity in the response can be observed when measuring with high voltage allowing single-photon sensitivity.

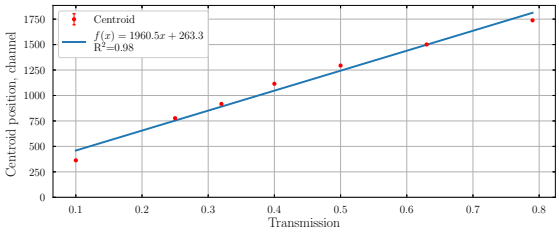

Figure 15: Peak centroid position vs. light intensity for the R7600U PMT at +850 V. The spectrum range is 4096 channels.

As in the previous case of the H11934 PMT, linearity of the PMT response is recovered by decreasing the high voltage supplied to the PMT, avoiding saturation in the divider response. The results are presented in Fig. 16, where excellent linearity is observed.

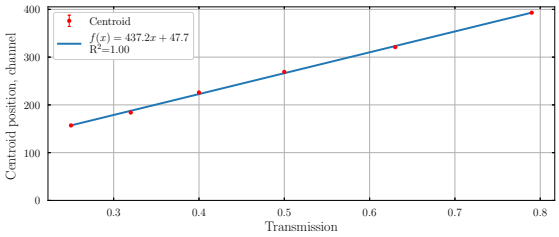

Figure 16: Peak centroid position vs. light intensity for the R7600U PMT at +720 V. The spectrum range is 512 channels.

However, the non-uniformity of the photocathode response again introduces significant spread of the experimental points. This is shown in Fig. 17 where measurements on random points at the photocathode result in notable spread of the response for each filter.

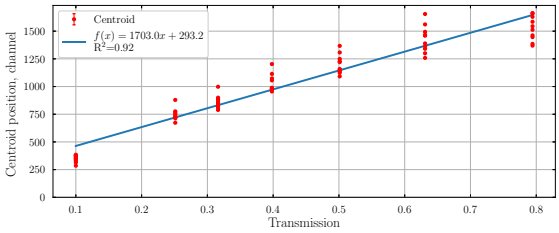

Figure 17: Peak centroid position vs. light intensity for the R7600U PMT at +850 V. Points corresponding to the same optical transmission are measured on ten different random positions in the effective area of the photocathode. The spectrum range is 4096 channels.

3.3. Influence of the non-uniformity of the photocathode response on alpha-spectra

The PSF200A plastic scintillator with ^{222}Rn absorbed in it was used for the purpose of this investigation. Two separate exposures to air with high (∼100 MBq/m3) ^{222}Rn concentration of the same PS piece were made for the measurements with the H11934 and R7600U PMTs. The settings of the nanoPSD are set to automatic thresholds and the software range of the alpha-spectrum was set to 512 channels. The frame of reference used for the measurements with the PS is the one shown in Fig. 4 left. The focusing electrodes are parallel to the Y axis. In Fig. 4 left, the number of the columns/rows of the grid is indicated on the X/Y axis and this notation is used in the figures below.

The alpha-spectrum of ^{222}Rn and its decay products is obtained after pulse-shape discrimination. The nanoPSD analyzer provides four spectra: TIPS spectrum, the raw alpha and beta spectrum and the separated alpha and beta spectra. The spectra for a PS in the center of the PMT show good separation of the pulses of alpha and beta particles (Fig. 5). This enables us to investigate the TIPS and alpha spectra and follow the changes in them when placing the PS in different points on the photocathode of the PMT.

3.3.1. Hamamatsu H11934-203 PMT

Figures 18 and 19 present the TIPS and the alpha spectra measured with the H11934 PMT. The high voltage supply was set to +750V. The spectra

are acquired by consequently placing and measuring the PS in the openings of the grid (Fig. 4). The acquisition time is adjusted according to the counting statistics.

Figure 18 shows the TIPS spectra obtained at different positions on the PMT photocathode. In order to evaluate the effect of the non-uniformity on the pulse-shape discrimination we use a figure of merit (FOM) defined as the difference between the maxima of two peaks divided by the sum of the FWHM of the peaks. The FOM is estimated by an algorithm available in the nanoPSD software.

From Fig. 18 it can be seen that the FOM in the center of the grid is higher compared to the outer spectra. This indicates that, indeed, the non-uniformity of the photocathode response has an influence on the pulse-shape discrimination. Although the FOM parameter is not affected by the non-uniformity as much as the energy resolution, it definitely repeats the variation observed in the energy resolution (see Fig. 19).

In Fig. 19 it can be noted that in the center of the photocathode, the energy resolution is good enough and allows separation of the maxima of the α-peaks of ^{222}Rn and ^{218}Po. This is not the case for the outer positions and especially in the corners where the quantum efficiency of the photocathode is low. There is also a notable difference between the spectra in the first and last columns with the former having higher energy resolution. Possible explanation for that is the higher quantum efficiency (high centroid position) in the part of the PMT where Y $>$ 15 mm (see Fig. 8). The influence of the non-uniformity on the shape of α-peaks was studied in [7] by measuring PS pieces of different sizes.

3.3.2. Hamamatsu R7600U-200 PMT

Figures 20 and 21 show the TIPS and the alpha spectra obtained with the Hamamatsu R7600U PMT. The grid position is the same as for the H11934 PMT but the high voltage supply is set to +720 V.

Figure 20 shows the TIPS spectra obtained at different positions on the PMT. It can be seen that compared to the H11934 PMT there is a greater

variance in the FOM value between the spectra. Furthermore, in the corners of the PMT window, the PSD is so degraded that the FOM cannot be estimated. This is explained by the much smaller effective area of the R7600U-200 PMT.

Similarly to the measurements with the H11934 PMT, the maxima of ^{222}Rn and ^{218}Po peaks are separated only in the center of the PMT (Fig. 21). Moreover, the peak of ^{214}Po alpha particles is also not separated in the outer spectra. This could be explained by the fact that except in the four central positions, for all other positions the PS piece is outside the effective area of the PMT.

It should be noted here that the effects observed when the ^{222}Rn-loaded PS was placed at the outer positions of the grid are due not only to the PMT non-uniformity, but also to the fact that a part of the PS faces the inactive part of the PMT (see Fig. 4). The results demonstrate that such situations are highly undesirable and special care to cover the inactive parts of the PMT must be taken when constructing the optical chamber of the counters.

4. Discussion on the effect of PMT spatial non-homogeneity on measurement methods using the free parameter model

The free parameter model is used in radionuclide metrology for the direct calibration of the activity of radionuclides [12]. In this model, the Poisson distribution of the number of photons emitted by the scintillation light pulse is traditionally used to calculate the detection efficiency from the non-detection efficiency, i.e., the probability that no photoelectron is detected. In case of a spatial non-uniformity of the PMT response, the mean value of the Poisson distribution, describing the intrinsic light yield of the detection process, is no more a constant value but becomes a random variable with a distribution affected by the fluctuations of the detection process, which leads to a compound Poisson distribution. The non-detection efficiency calculation is similar to the one using a Poisson distribution, but its uncertainty is larger, due to the variability of the random variable describing the mean value of the compound Poisson distribution. This effect leads to an increased uncertainty on the detection efficiency,

especially when measuring low-energy radionuclides or when the detection efficiency is reduced.

The non-uniformity of the photocathode response is a possible explanation for the problems observed in the Triple to Double Coincidence Ratio (TDCR) measurements when reducing the detection efficiency [21].

A possible solution to the non-uniformity of the PMT response would be to mask the most effective area of the PMTs which, in turn, equalizes the quantum efficiency of the photocathode. This idea has previously been explored in [22–24], but has a major drawback, which is the decrease of the photon detection probability. According to our experience, the best approach to minimize the non-uniformity is to mask carefully the ineffective area of the PMTs. In addition, for TDCR measurements it is important to include the PMT non-homogeneity in the calculation model in order to account for the larger detection uncertainty.

5. Conclusions

In this work we have developed an experimental system to study the effects of the non-uniformity of the PMT response on the scintillation counting measurements. This effect has been described and quantified for scintillation detectors using Hamamatsu R7600U-200 and H11934-203 PMTs.

We identified a degradation of the counting efficiency and the energy resolution both in the effective area and at the periphery of the PMTs. The relatively large ineffective area of the R7600U-200 PMT causes significant problems in scintillation counting as it acts as a photon sink. The H11934 PMT has a smaller ineffective area but it also has to be masked with reflective foil in order to reduce the variance in scintillation counting experiments.

It has been shown that the non-uniformity of the PMT response has an adverse effect on the energy resolution of scintillation spectrometry and the pulse-shape discrimination. The effects of the non-uniformity of the PMT response regarding the radionuclide activity measurements using the free param-

eter model are discussed.

6. Acknowledgments

This work is supported by the Bulgarian National Scientific Research Fund under contract KP-06-H38/9 from 06.12.19 (TDCX).

References

[1] T. F. Godlove, W. G. Wadey, Photocathode uniformity and resolution of scintillation spectrometers, Review of Scientific Instruments 25 (1) (1954) 1–4. doi:10.1063/1.1770874.
URL https://doi.org/10.1063/1.1770874

[2] B. Leskovar, C. C. Lo, Performance studies of photomutipliers having dynodes with GaP(cs) secondary emitting surface, IEEE Transactions on Nuclear Science 19 (3) (1972) 50–62. doi:10.1109/tns.1972.4326702.
URL https://doi.org/10.1109/tns.1972.4326702

[3] G. F. Knoll, Radiation detection and measurement, Wiley, 1989.
URL https://books.google.bg/books?id=dyBRAAAAMAAJ

[4] A. W. Schardt, W. Bernstein, Resolution of the scintillation spectrometer, Review of Scientific Instruments 22 (12) (1951) 1020–1021. doi:10.1063/1.1745805.
URL https://doi.org/10.1063/1.1745805

[5] P. S. Takhar, Resolution and cathode uniformity in scintillation counters, IEEE Transactions on Nuclear Science 14 (1) (1967) 438–442. doi:10.1109/tns.1967.4324451.
URL https://doi.org/10.1109/tns.1967.4324451

[6] M. Mottaghian, R. Koohi-Fayegh, N. Ghal-Eh, G. R. Etaati, Photocathode non-uniformity contribution to the energy resolution of scintillators, Radiation Protection Dosimetry 140 (1) (2010) 16–24. doi:10.1093/rpd/

ncq041.
URL https://doi.org/10.1093/rpd/ncq041

[7] V. T. Todorov, C. C. Dutsov, P. Cassette, K. K. Mitev, Effects of the photocathode non-uniformity on radon measurements by plastic scintillation spectrometry, Journal of Radioanalytical and Nuclear Chemistrydoi:10.1007/s10967-022-08362-6.
URL https://doi.org/10.1007/s10967-022-08362-6

[8] H. Kume, S. Sawaki, M. Ito, K. Arisaka, T. Kajita, A. Nishimura, A. Suzuki, 20 inch diameter photomultiplier, Nuclear Instruments and Methods in Physics Research 205 (3) (1983) 443–449. doi:10.1016/0167-5087(83)90007-8.
URL https://doi.org/10.1016/0167-5087(83)90007-8

[9] M. U. Elorrieta, R. Busse, L. Classen, A. Kappes, Homogeneity of the photocathode in the hamamatsu r15458-02 photomultiplier tube, Journal of Instrumentation 16 (11) (2021) P11038. doi:10.1088/1748-0221/16/11/p11038.
URL https://doi.org/10.1088/1748-0221/16/11/p11038

[10] F. Gao, S. Qian, Y. Ma, J. Xia, Z. Ning, Z. Wang, L. Ma, Q. Wu, S. Peng, Research and development of 20-inch PMT uniformity scanning platform, Nuclear Instruments and Methods in Physics Research Section A: Accelerators, Spectrometers, Detectors and Associated Equipment 1027 (2022) 166257. doi:10.1016/j.nima.2021.166257.
URL https://doi.org/10.1016/j.nima.2021.166257

[11] J. Paul, Studies concerning the behaviour of photomultiplier with large photocathode, Nuclear Instruments and Methods 89 (1970) 285–287. doi:10.1016/0029-554x(70)90836-0.
URL https://doi.org/10.1016/0029-554x(70)90836-0

[12] R. Broda, P. Cassette, K. Kossert, Radionuclide metrology using liquid scintillation counting, Metrologia 44 (4) (2007) S36.

[13] Hamamatsu r7600u-200 photomultiplier tube datasheet, [Online; accessed 1-August-2022].
URL https://www.hamamatsu.com/content/dam/hamamatsu-photonics/sites/documents/99_SALES_LIBRARY/etd/R7600U_TPMH1317E.pdf

[14] Hamamatsu h11934-203 photomultiplier tube datasheet, [Online; accessed 1-August-2022].
URL https://www.hamamatsu.com/content/dam/hamamatsu-photonics/sites/documents/99_SALES_LIBRARY/etd/R11265U_H11934_TPMH1336E.pdf

[15] R. Kossakowski, J. Audemer, J. Dubois, D. Fougeron, R. Hermel, R. Sottile, J. Vialle, Study of the photomultiplier R7600-00-M4 for the purpose of the electromagnetic calorimeter in the AMS-02 experiment, Tech. rep. (2002).
URL http://hal.in2p3.fr/in2p3-00021475

[16] Real-time digital pulse-shape discriminator (psd) and spectrometer with simultaneous amplitude and pulse-shape discrimination, https://www.yantel.com/products/nanopsd/.

[17] K. Mitev, V. Jordanov, M. Hamel, C. Dutsov, S. Georgiev, P. Cassette, Development of a portable scintillation spectrometer with alpha-/beta- and neutron-/gamma- pulse-shape discrimination capabilities, in: 2018 IEEE Nuclear Science Symposium and Medical Imaging Conference Proceedings (NSS/MIC), IEEE, 2018. doi:10.1109/nssmic.2018.8824692.
URL https://doi.org/10.1109/nssmic.2018.8824692

[18] V. T. Jordanov, Pile-up real time pulse-shape discrimination based on ballistic deficit measurement and digital time-invariant pulse shaping, in: 2018 IEEE Nuclear Science Symposium and Medical Imaging Conference Proceedings (NSS/MIC), IEEE, 2018. doi:10.1109/nssmic.2018.8824502.
URL https://doi.org/10.1109/nssmic.2018.8824502

[19] Hamamatsu photonics, Photomultiplier tubes - basics and applications (2017).
URL https://www.hamamatsu.com/resources/pdf/etd/PMT_handbook_v4E.pdf

[20] V. Simeonov, G. Larcheveque, P. Quaglia, H. van den Bergh, B. Calpini, Influence of the photomultiplier tube spatial uniformity on lidar signals, Applied Optics 38 (24) (1999) 5186. doi:10.1364/ao.38.005186.
URL https://doi.org/10.1364/ao.38.005186

[21] P. Arenillas, P. Cassette, Implementation of the TDCR liquid scintillation method at CNEA-LMR, argentina, Applied Radiation and Isotopes 64 (10-11) (2006) 1500–1504. doi:10.1016/j.apradiso.2006.02.091.
URL https://doi.org/10.1016/j.apradiso.2006.02.091

[22] A. Dean, N. Dipper, R. Lewis, L. Z. Guo, F. Perotti, A diffusive light collection system for hard x-ray astronomical scintillation detectors, Nuclear Instruments and Methods in Physics Research Section A: Accelerators, Spectrometers, Detectors and Associated Equipment 236 (2) (1985) 410–413. doi:10.1016/0168-9002(85)90185-8.
URL https://doi.org/10.1016/0168-9002(85)90185-8

[23] J. Veloso, J. dos Santos, C. Conde, Large-window gas proportional scintillation counter with photosensor compensation, IEEE Transactions on Nuclear Science 42 (4) (1995) 369–373. doi:10.1109/23.467818.
URL https://doi.org/10.1109/23.467818

[24] J. Mead, J. Martin, Improvement of resolution in large area photomultipliers, Nuclear Instruments and Methods 36 (1965) 13–22. doi:10.1016/0029-554x(65)90400-3.
URL https://doi.org/10.1016/0029-554x(65)90400-3

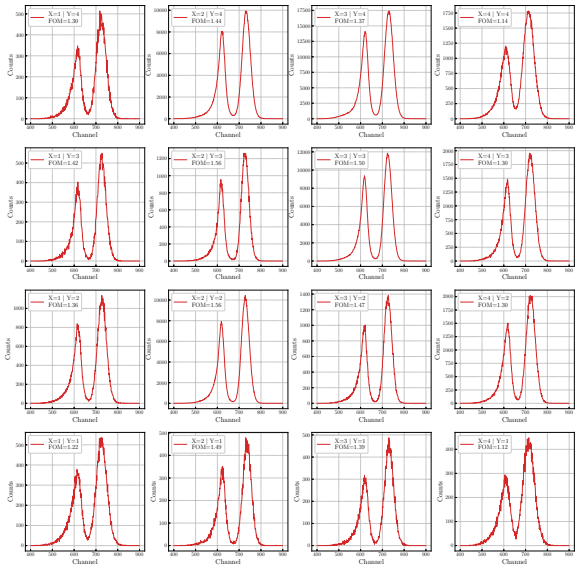

Figure 18: TIPS spectra of ^{222}Rn absorbed in PSF200A obtained at different positions on the photocathode of H11934-203 PMT. The estimated FOM of each spectrum is given in the legend.

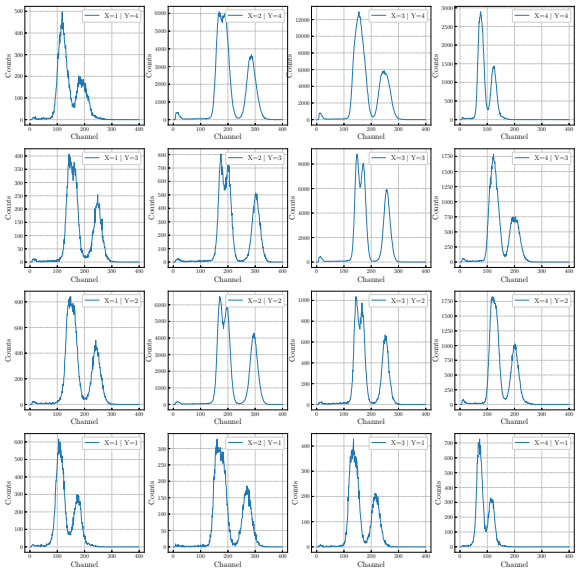

Figure 19: Pulse-height alpha spectra corresponding to the measurements shown in Fig. 18.

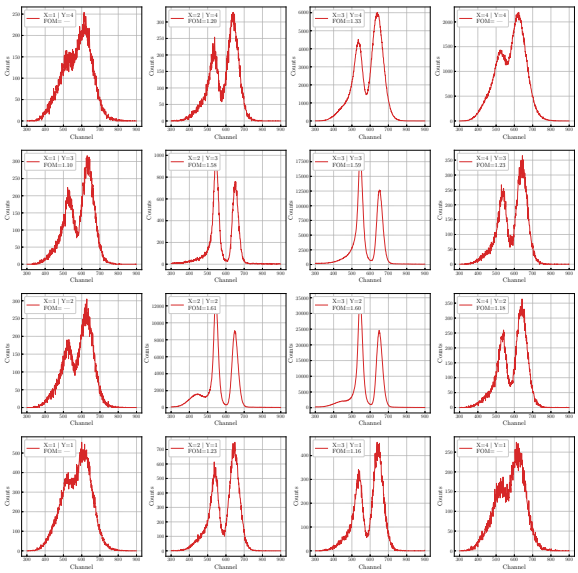

Figure 20: TIPS spectra of ^{222}Rn absorbed in PSF200A obtained at different positions on the photocathode of R7600U-200 PMT. The estimated FOM of each spectrum is given in the legend.

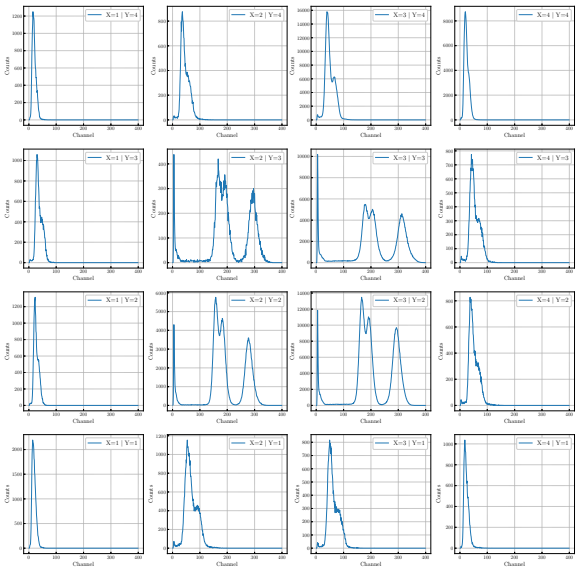

Figure 21: Pulse-height alpha spectra corresponding to the measurements shown in Fig. 20.